The Interplay of Intra- and Intermolecular Interactions in Solid Iodine at Low Temperatures: Experimental and Theoretic Spectroscopy Study

I.D. Yushina*[1] B.A. Kolesov[2,3]

[1]*South Ural State University, Chelyabinsk, Russia*

[2]*A.V. Nikolaev Institute of Inorganic Chemistry, Siberian Branch, Russian Academy of Sciences, Novosibirsk, Russia*

[3]*Novosibirsk National State Research University, Faculty of Physics, Russia*

E-mail: iushinaid@susu.ru

Abstract

This work is devoted to the discussion of structural changes in crystalline iodine under low temperature studied from experimental and theoretic points of view. Experimental Raman spectra in the temperature range 5 K – 300 K demonstrated unusual behavior of stretching vibration at ~180 cm^{-1} with temperature. The data allowed obtaining of $\omega(T)$ functions for both external translational and internal stretching modes of I_2. It was found that $\omega(T)$ trends significantly differ in comparison to typical van-der-Waals crystal α-S_8. Observed anomalies are explained from a theoretic point of view due to the strengthening of intralayer halogen bonding between I_2 molecules.

Introduction

Recent studies in the field of chemical bonding show the exponential growth of the number of publication, devoted to the study of halogen bonding.[1] As defined by IUPAC[2] halogen bonding is the attractive interaction in which a halogen atom provides its electrophilic region for bonding. This effect is essential in case of crystal engineering of halogen-containing materials.[3] The effect of halogen bonding had been thoroughly studied previously from electron density point of view in the series of the works.[4, 5]

The crystalline iodine itself represents a nice model example for halogen bonding studies as it demonstrates the highest atomic polarizability in the halogen row due to the largest van-der-Waals radius and thus the most evident anisotropy of electrostatic potential on the electron density isosurface.[6, 7] Let us consider the

fundamental interactions which are presented in the crystal structure of solid iodine. Schematic presentation of considered interactions is shown in Fig. 1 according to experimental X-Ray data.[8] The two main intermolecular interactions here are as follows: the intralayer bond which is usually called as halogen bond (XB) with the distance 3.501 Å and the interlayer long-range I…I van der Waals interaction with distance 4.280 Å. Such notation will be further used through the present work.

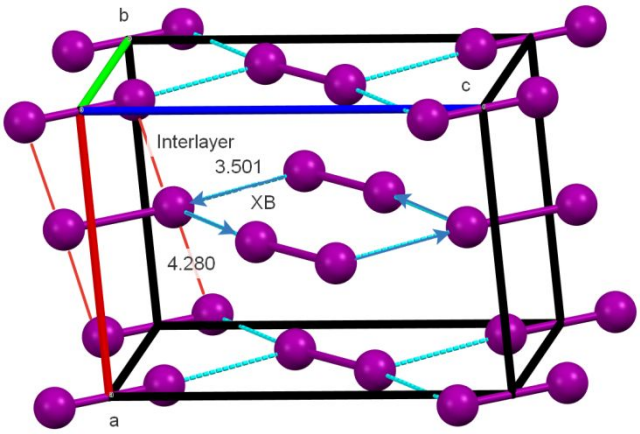

Fig. 1 Crystal packing of iodine crystal with shown distances and types of intermolecular interactions according to[8]

The crystal structure and spectral properties of crystalline iodine had been studied using different experimental techniques under various external conditions.[8–11] It was previously reported that under hydrostatic pressures above 23 GPa iodine demonstrates the transition to monoatomic phase so that all the atoms in the layer become indistinguishable and the intra- and intermolecular distances become equal to each other (2.965 Å).[9, 10]

The spectroscopic studies of iodine are often focused on the behavior of intramolecular I_2 stretching modes but low-frequency bands of intermolecular vibrations usually remain beyond consideration. However simultaneous consideration of all vibration bands together with the observation of their dependencies with temperature can give valuable quantitative information about the interplay between intra- and intermolecular interactions.[9, 11]

Recent studies show the anomalous spectral and structural behavior of bromine under high pressures according to experimental and computational data.[12] Non-monotonous change of Br…Br intermolecular distance was interpreted from the point of the influence of intermolecular interactions, although qualitative understanding of these effects had not been found.

Here we perform the attempt not only to experimentally examine the changes in iodine structure under low temperatures, but also to identify theoretically the root electronic properties which cause these changes.

Experimental

Single crystal Raman spectra were collected on a LabRAM Horiba single spectrometer with a CCD Symphony (Jobin Yvon) detector that provided 2048 pixels along the abscissa. The laser line was used for the wavenumber correction of the spectra. The laser power (633 nm line of He-Ne laser) at the sample was typically 1 μW. The spectra at all temperatures were measured in backscattering collection geometry with a Raman microscope. The crystals were wrapped in indium foil for better thermal contact, keeping an open area at the upper surface accessible for light, and fixed on a cold finger of the closed cycle He-cryostat (ARS Optical Cryostat DE210AF-GMX-20-OM). All measurements were performed with a spectral resolution of 0.7 cm^{-1}.

Calculations

Periodic Kohn-Sham calculations were performed in CRYSTAL17 package[13] using B3LYP-D*[14,15] functional with dispersion correction.[16,17] Structure optimizations were done under predefined external hydrostatic pressure in the range 0-6 GPa using 8x8x8 k-points net. The modified DZVP set for iodine atom was applied[18], see supplementary section. Truncation criteria for bielectronic integrals have been set as follows: overlap threshold for Coloumb integrals and Hartree-Fock exchange integrals equals 10^{-10} a. u., penetration threshold for Coloumb integrals is 10^{-10} a. u.; the first and second criteria for pseudo-overlap are 10^{-10} and 10^{-16} a. u., respectively, these values are higher than the default ones in order to control better quality of calculations. The positions of Raman active modes were calculated for all pressure points according to couple-perturbed Kohn-Sham methodology.[19] No negative modes were observed in Hessian matrix in discussed pressure range with above-mentioned level of theory. The initial structure of crystalline iodine was also optimized in different ways under ambient conditions, the results are presented in Table 1.

Table 1 Raman active modes (cm^{-1}) using different calculation methods, the values in the brackets correspond to the difference Δ between experimental and calculated data

	δ interlayer	δ intralayer (XB)	υ_{as}	υ_{s}
B3LYP, ao*	63.8 (11.2)	85.2 (0.8)	178.6 (1.4)	187.4 (1.6)
B3LYP-D, ao*	59.0 (16)	93.9 (-7.9)	175.7 (4.3)	187.3 (1.7)
B3LYP-D, cv*	69.6 (6.4)	84.9 (1.1)	181.0 (1)	189.9 (0.9)
B3LYP-D, cell*	55.9 (20.1)	69.4 (16.6)	182.7 (2.7)	189.5 (0.5)
B3LYP-D3, cv	60.9 (14.1)	82.0 (4.0)	178.0 (2.0)	186.2 (2.8)
M-06, cell*	56.1 (19.9)	74.0 (12)	214.1 (34.1)	214.1 (25.1)
Mean Δ, cm^{-1}	14.7	7.7	8.7	6.0
Mean Δ, B3LYP-D, cm^{-1}	13.4	6.6	4.7	1.2

*ao - optimization with fixed cell parameters and allowed shift of only atomic positions;
cv- optimization with constant volume;
cell – optimization with simultaneous change of cell parameters and atomic position so that overall symmetry does not change.

The lowest mean delta value is observed for B3LYP-D*,mod-DZVP, cv optimization – 2.4 cm^{-1} over all four bands, with the highest Δ contribution due to underestimation of the position of the interlayer band. The main methodological question here is how to correctly reproduce the data for the bands due to intermolecular interaction with the high dispersion component. As we can see the direct account of it in M-06 functional[20] leads to unacceptable results thus the most reasonable way is to treat dispersion on the level of Grimme corrections on the basis of functional which best reproduces the valence band position. Quantum-topological analysis of electron density was performed in TOPOND using the wave function data.[21, 22]

Results and Discussion

Experimental Raman spectrum at 5 K is presented on Fig. 2. Here one can see two translational modes at 75 and 86 cm^{-1} and two valence modes at 180 and 189 cm^{-1}. According to theoretic interpretation, the first two bands correspond to translational vibrations of the molecules between layers (75 cm^{-1}) and within one crystal layer (86 cm^{-1}) correspondently. The latter bands refer to stretching vibrations of covalently bound I-I molecule, symmetric in-phase ν_s, 189 cm^{-1} and asymmetric out-of-phase ν_{as}, 180 cm^{-1}.

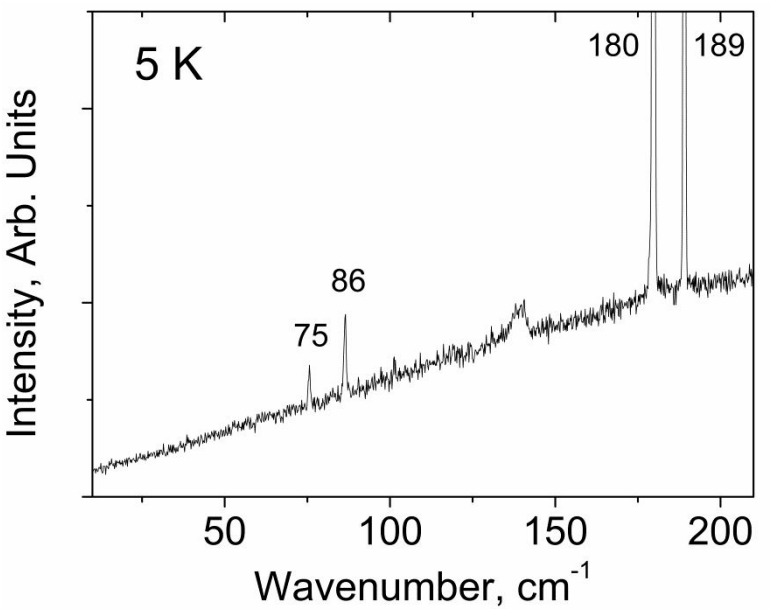

Fig. 2 Experimental Raman spectrum of iodine at 5 K

Fig. 3a-d represents the dependency of peak positions of observed modes with temperature. The solid curves for ω(*T*) at Fig. 3a-b are drawn according to the equation:

$$\omega(T) = \omega(0) + A\langle n(\omega,T)\rangle, \quad (1)$$

where $\langle n(\omega,T)\rangle$ - is the mean value of the vibrational quantum number, defined as Plank`s equation. The output of equation (1) can be found in the previous work.[23] The numerical value of anharmonicity coefficient *A* in (1) indicates how the mode wavenumber varies with the change of vibrational quantum number of the oscillator by unity, i.e. from $\langle n\rangle = 0$ to $\langle n\rangle = 1$, from $\langle n\rangle = 1$ to $\langle n\rangle = 2$ and so on under corresponding temperatures. In other words, the *A* value equals the magnitude of anharmonic contribution into the ω vibration when thermally excited.

ω(*T*) dependency of modes at 180 and 189 cm^{-1} demonstrate anomalous behavior. For this reason, solid curves describing the ω(*T*) function of phonons at 180 and 189 cm^{-1} are related to thermal occupancies not these particular phonons but refer to translational mode at 86 cm^{-1} in crystal (see below). They show that the wavenumbers of both valence modes depend on the characteristics of intermolecular interactions.

Above mentioned ω(*T*) curves on Fig. 3a-b significantly differ from the ones observed for typical molecular crystals. Hereby anharmonic coefficients *A* for translational modes at 75 and 86 cm^{-1} are several times higher than in translational modes in typical van-der-Waals crystal α-S_8.

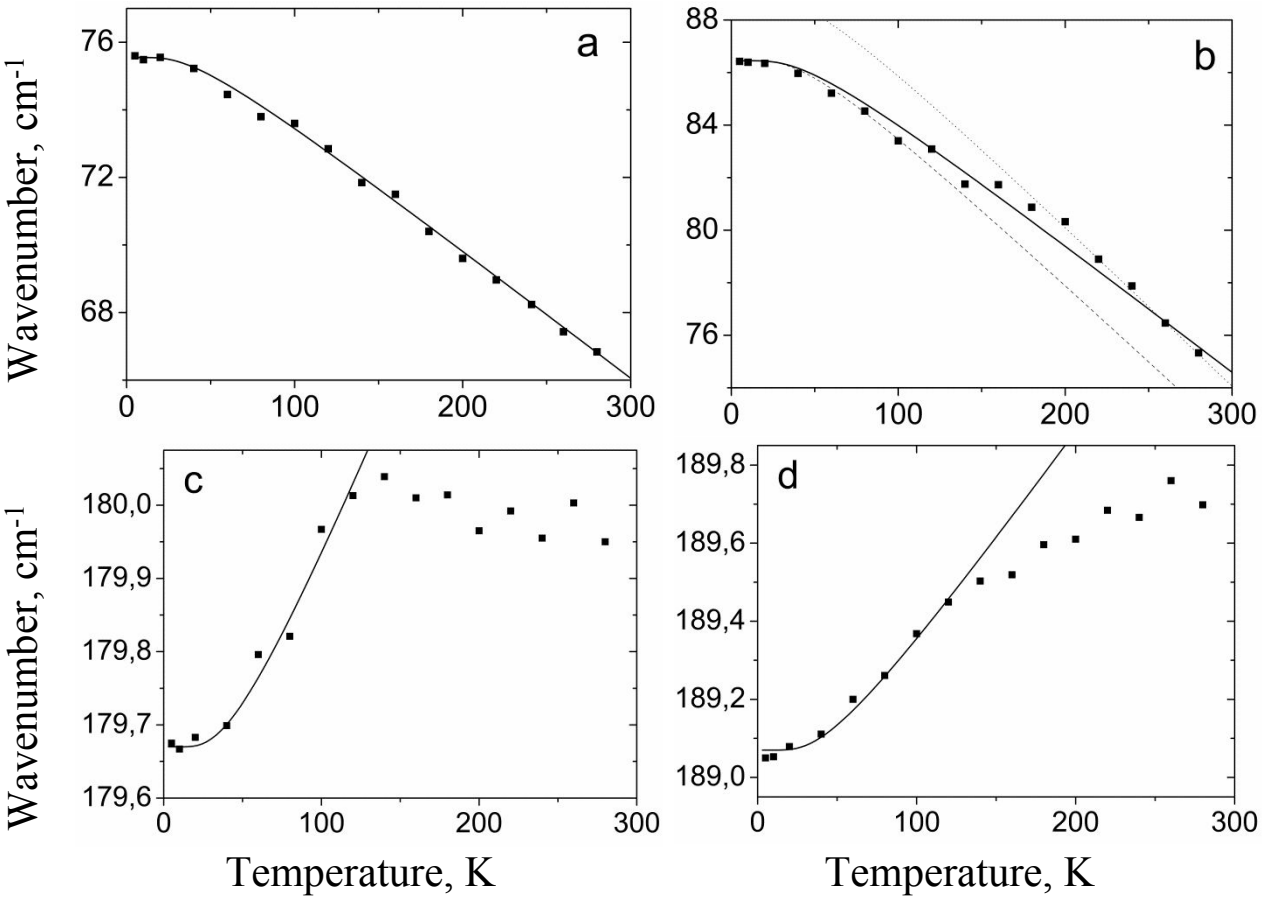

Fig. 3 The experimental dependency of maxima position of the translational (a, b) and stretching (c, d) vibration modes with temperature. A detailed description of fitting parameters can be found in the text. Dependency of 86 cm^{-1} (b) mode permits different fitting in low- (dotted) and high-temperature (dashed) regions.

In Table 2 we compare the *A* values for comparable in frequency translational modes of both I_2 and α-S_8 crystals. All values have been obtained in the present work. Raman spectra of α-S_8 were presented elsewhere.[24] It can be seen that translational modes in iodine crystal change with temperatures 2-4 times faster than in sulfur crystal. This means that the intermolecular interactions of I_2 molecules have not only prominent van der Waals component but also a significant effect of polarization which was postulated previously on the basis of gas-phase calculations. This is exactly the effect which is usually attributed in the literature to the emergence of specific halogen bond based on string electrostatic component due to the anisotropy of electrostatic potential distribution on the electron density isosurface.[25]

The most unusual behavior is demonstrated by $\omega(T)$ dependency of valence modes at 180 and 189 cm^{-1}. Instead of expected increase of wavenumber with decrease of temperature, these modes manifest anomalous decrease of wavenumber (fig. 3c-d). Usually decrease of temperature means freezing of the

vibrations, decrease of their root-means-square amplitude and I-I distance resulting in the strengthening of the covalent bond.

Table 2 Experimental wavenumbers (at 5 K) and anharmonic coefficients *A* of vibration modes in crystals of I_2 and α-S_8.

	I_2		α-S_8										
ω, cm^{-1}	75	86	31	32	45	53	54	60	64	69	77	85	91
A, cm^{-1}	4.15	6.1	0.285	0.85	0.5	1.26	0.9	2.1	0.5	1.4	0.7	1.4	1.82

In order to understand above-mentioned anomalies and to find their origins we performed solid state quantum-chemical calculations with periodic boundary conditions for I_2 crystal. In the attempt to reproduce dynamic character of obtained experimental spectral data with temperature, we made calculation under external hydrostatic pressures to obtain the series of structures with various structural characteristics and spectral data. Following this strategy we able to obtain computational dependencies of bond length and intermolecular distances, wavenumbers of valence and translational vibrations comparable with experimental data. Such computational strategy had been chosen because of significant difficulties in modeling temperature changes thus structural changes observed in the experiment were reproduced in calculations with external hydrostatic pressures.

The change of theoretical I-I distance in the range 0–3 GPa of external pressure (fig. 4) is in good agreement with experimental spectral data for stretching vibration (fig. 3c), where at the beginning the frequency is slightly increasing on cooling and then starts decreasing. It is in agreement with the well-known observation that in molecular crystals the change of structural parameters on cooling from ambient temperature to cryogenic conditions usually corresponds to the pressure range 2-3 GPa. Thus only the starting section of the calculated pressure curve is significant for the comparison with experimental spectral data under low temperatures.

On the increase of pressure from 1 to 3 GPa the I–I bond length is not decreasing as it could be expected, but increases. Similar dependency has been recently discovered for the case of Br–Br distance for Br crystals.[12] Similar observations were previously reported in high-pressure experiments with solid iodine according to single crystal X-ray diffraction data[26] and with liquid iodine

according to X-ray absorption spectroscopy data.[27] Thus, ω(*T*) for stretching modes of I-I vibrations (Fig. 3c-d) is highly correlated with the calculated data (fig. 4) if we compare temperature range 300 K – 5 K with pressure range 0 – 3 GPa.

Intramolecular characteristics, i.e. vibrational frequency and bond length as a function of temperature (Fig. 3c-d) and external pressure (Fig. 4) respectively, show anomalies while corresponding intermolecular parameters change linearly (Fig. 5). It proves the hypothesis that the intermolecular interactions in I_2 and Br_2 crystals are significantly more complicated than just Van-der-Waals interaction and includes additional polarization component which becomes evident in some edge conditions: i.e. at approximately 1 GPa in pressure (Fig. 4) and 100-150 K in temperature (Fig. 3c-d).

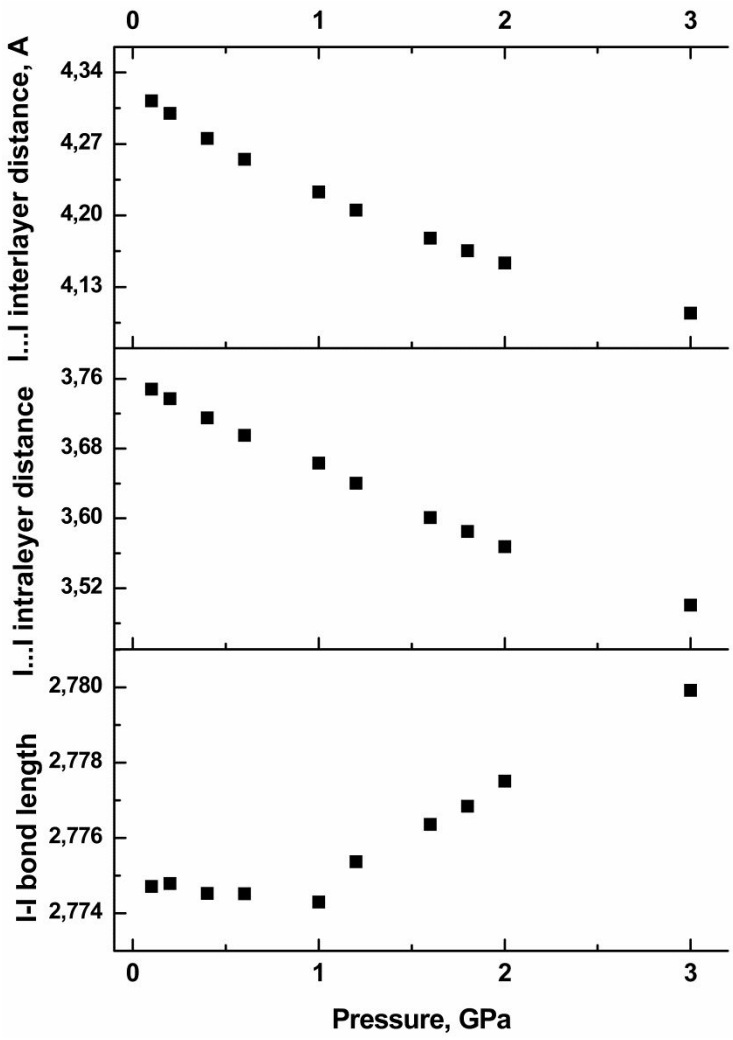

Fig. 4 Calculated dependency of I–I/I…I distances (Å) over external pressure for interlayer van der Waals interaction (up), intralayer halogen bond (center) and covalent bond (down)

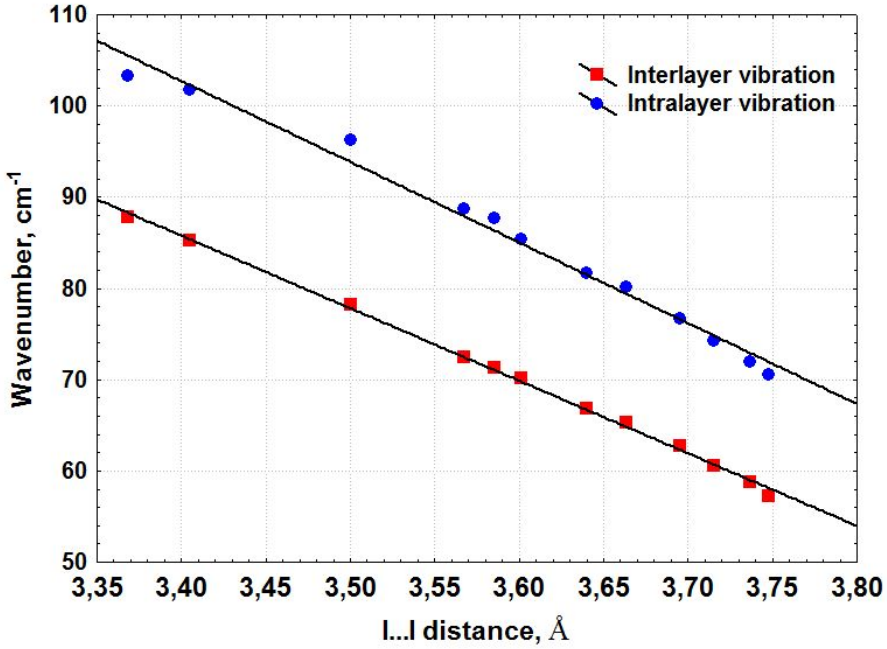

Fig. 5 Calculated dependency of the wavelength of intra- and interlayer I…I vibrations over the change of I…I distances with pressure. The increase of external pressure goes from right side to the left.

The strengthening of intermolecular interaction together with the weakening of covalent bond in the crystals of I_2 and Br_2 is observed in the experiment on cooling and in theory on increase of external pressure up to 3 GPa. Thus it is worth describing this interplay phenomenon on quantum-chemical level and search for electronic parameters which can reveal the quantitative interrelation between the frequency of valence and translational modes as well as I-I lengths and I...I distances. Electron density of covalent bond is insufficiently representative for such tasks as it does not show significant differences for such low changes in I-I bond length in the range 0 – 3 GPa corresponding to the conditions of the experiment and besides does not exhibit linear correlation with experimental spectral data. If we compare this observation with the charge density data for bromine,[12] we see that the authors identify significant changes in the 2D distribution of electron density within crystal layer only for pressure above 5.4 GPa which is much higher than we can directly compare with low-temperature data.

However, we found that electron localization function (ELF) value in the bond critical point of electron density for I–I covalent bond can uniformly determine and predict the position of both stretching and translational bands and the dependency in this case is clearly linear: R^2 = 0.980 for interlayer vibration, 0.981 for intralayer, 0.995 for υ_{as} vibration (fig. 6a).

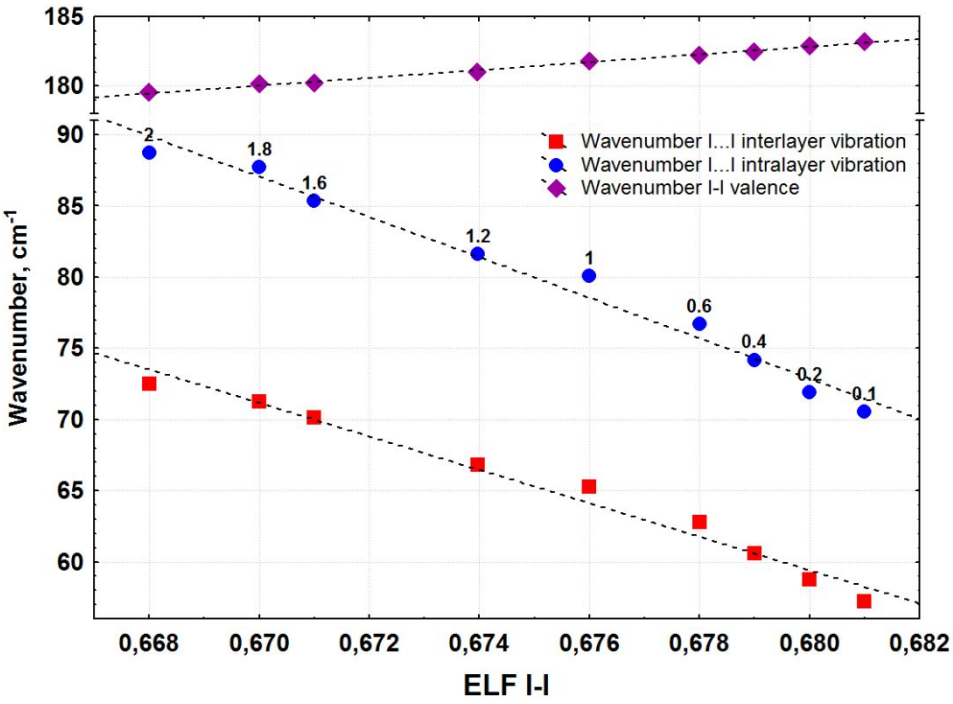

(a)

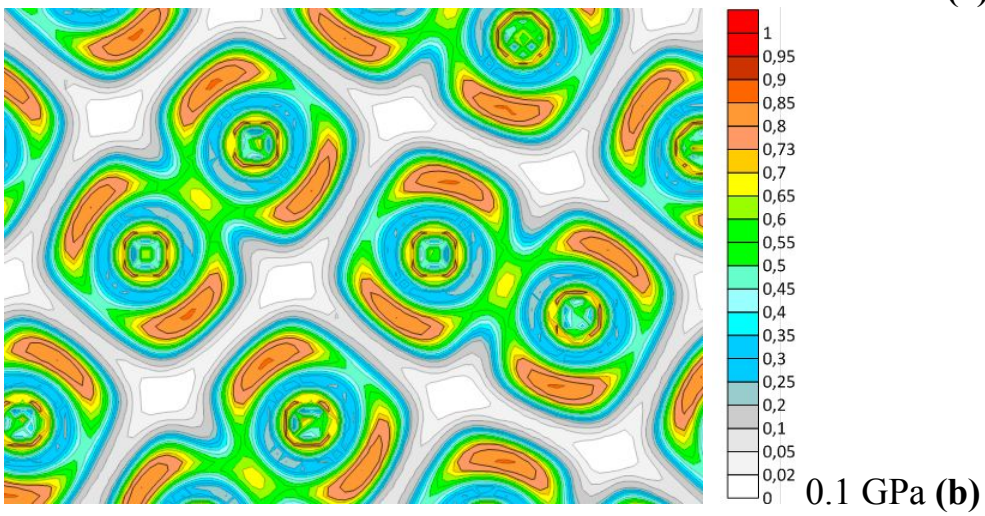

0.1 GPa **(b)**

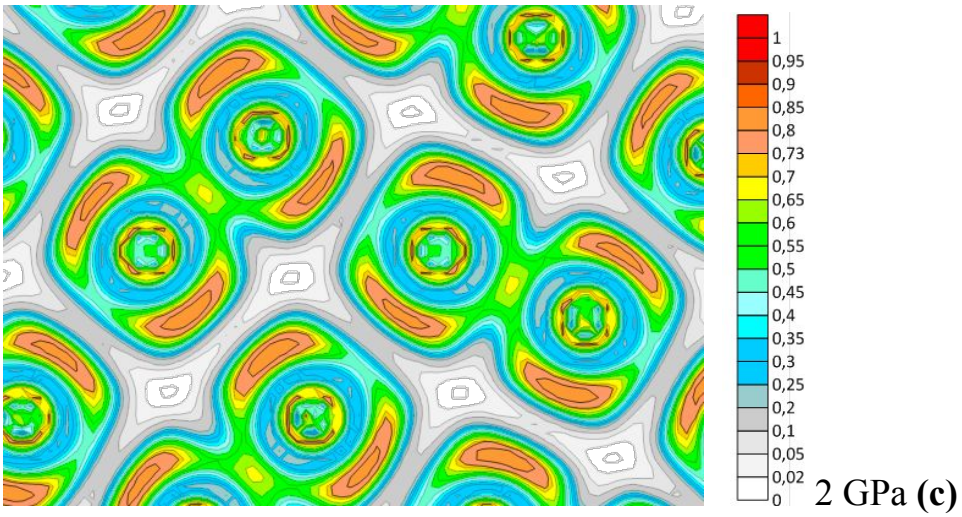

2 GPa **(c)**

Fig. 6: a) Interrelation between ELF value in the bond critical point of electron density for I-I covalent bond and the calculated position of stretching and translational modes, the pressure decreases from right to the left as it is shown near the dots of halogen bond vibration (blue); Distribution of ELF values in the *bc* crystal plane at 0.1 (b) and 2 (c) GPa

This observation can be explained on the basis of physical meaning and definition of ELF: it represents the degree of electron localization revealing the regions of electron accumulation.[28, 29] As it is a relative scale normalized in the range from 0 to 1, where 1 corresponds to perfectly localized electron and 0.5 refers to the delocalized electron gas. It was previously noticed, that ELF values for I-I bond above 0.5 correspond to the existence of bound molecular iodine as a subunit in complex polyiodide systems, while for I-I bond in triiodide ELF values are usually below 0.5.[4] At the same time special distribution of ELF function in the *bc* crystal plane (Fig. 6b-c) shows decrease of ELF values in the region of covalent bond (isoline 0.65, yellow) and in the region of lone-pairs in equatorial part of iodine atoms (isolines 0.8 and 0.85, orange) together with increase of values between I_2 molecules in the region of halogen bonds. The molecular and atomic character of different phases of iodine was previously studied using ELF.[30] Recently the role of ELF in prediction of compressibility in solids was also considered.[31] This theoretic interplay between covalent and halogen bond characteristics brings us closer to the understanding of both anomalous behavior of experimental stretching vibration band dependency with temperature (fig. 3c-d), as well as of high values of anharmonic coefficients in crystalline I_2 (Table 2). It also represents the structural trends which subsequently lead to the formation of atomic structure with indistinguishable covalent and halogen bond above 23 GPa.

Conclusions

The features of intra- and intermolecular interactions in the crystal structure of I_2 discussed in the present work are only the part of more general phenomenon when any strengthening if intermolecular interaction leads to weakening of intramolecular one. This empirical rule is usually well-proved on the examples of inclusion structures, in which host-guest interaction leads to low-wavenumber shift of intramolecular vibrations of guest bonds which are the most adjacent to the sub-cell of a host. One of the most common-known examples is the case of C–H vibrations in methane molecules in crystallohydrates. Their frequency is significantly lower in comparison to the frequency in unbound state and besides the more methane molecules there are in the cavity the stronger is the shift. This phenomenon still has no convincing justification. Taking into account the effects

of intermolecular interactions makes the observable frequency shifts quite reasonable.

Supplementary information Basis set description, illustration of dependency of covalent, halogen and interlayer I…I distances over external pressure, as well as thermal response properties obtained within quasi-harmonic approximation are presented in the Supplementary section.

Acknowledgements

IDY acknowledges support by the Ministry of Education and Science of the Russian Federation (grant No. 4.1157.2017/4.6); Government of the Russian Federation (Act 211, contract No. 02.A03.21.0011).

References

1 Cavallo, G.; Metrangolo, P.; Milani, R.; Pilati, T.; Priimagi, A.; Resnati, G.; Terraneo, G. The halogen bond. *Chem. Rev.* **2016**, *116*, 2478–2601. DOI: 10.1021/acs.chemrev.5b00484

2 Desiraju, G. R.; Ho, P. S.; Kloo, L.; Legon, A. C.; Marquardt, R.; Metrangolo, P.; Politzer, P.; Resnati, G.; Rissanen, K. Definition of the halogen bond. *Pure Appl. Chem*. **2013**, *85*, 1711−1713.

3 Priimagi, A.; Cavallo, G.; Metrangolo, P.; Resnati, G. The halogen bond in the design of functional supramolecular materials: recent advances. *Acc. Chem. Res*. **2013**, *46*, 2686–2695. DOI: 10.1021/ar400103r

4 Bartashevich, E.V.; Yushina, I.D.; Kropotina, K.K.; Muhitdinova, S.E.; Tsirelson, V.G. Testing the tools for revealing and characterizing the iodine-iodine halogen bond in crystals. *Acta Crystallographica* **2017**, *B73*, 217–226. DOI: 10.1107/S2052520617002931

5 Bartashevich, E.V.; Yushina, I.D.; Stash, A.I.; Tsirelson, V.G. Halogen bonding and other iodine interactions in crystals of dihydrothiazolo(oxazino)quinolinium oligoiodides from the electron-density viewpoint. *Crystal Growth & Design* **2014**, *14*, 5674–5684. DOI: 10.1021/cg500958q

6 Politzer, P.; Lane, P.; Concha, M. C.; Ma, Y. G.; Murray, J. S. An overview of halogen bonding. *J. Mol. Mod*. **2007**, *13*, 305–311.

7 Politzer, P.; Murray, J. S.; Clark, T. Halogen bonding: an electrostatically-driven highly directional noncovalent interaction. *Phys. Chem. Chem. Phys*. **2010**, *12*, 7748–7757.

8 Bertolotti, F.; Shishkina, A. V.; Forni, A.; Gervasio, G.; Stash, A. I.; Tsirelson, V. G. Intermolecular bonding features in solid iodine. *Crystal Growth & Design* **201**4, *14*, 3587–3595.

9 Kume, T.; Hiraoka, T.; Ohya, Y.; Sasaki, S.; Shimizu, H. High pressure Raman study of bromine and iodine: soft phonon in the incommensurate phase. *Phys. Rev. Lett*. **2005**, *94*, 065506.

10 Takemura, K.; Kyoko, S.; Hiroshi, F.; Mitsuko, O. Modulated structure of solid iodine during its molecular dissociation under high pressure. *Nature*, **2003**, *423*, 971–974.

11 Tassini, L.; Gorelli, F. A.; Ulivi, L. Far infrared phonons of solid iodine under pressure. *Chemical Physics Letters* **2003**, *378*, 105–110.

12 Wu, M.; Tse, J. S.; Pan, Y. Anomalous bond length behavior and a new solid phase of bromine under pressure. *Scientific Reports* **2016**, *6*, Article number 25649.

13 Dovesi, R.; Erba, A.; Orlando, R.; Zicovich-Wilson, C. M.; Civalleri, B.; Maschio, L.; Rerat, M.; Casassa, S.; Baima, J.; Salustro, S.; Kirtman, B. Quantum-mechanical condensed matter simulations with CRYSTAL. *WIREs Comput Mol Sci.* **2018**, *8*, e1360.

14 Becke, A.D. Density-functional exchange-energy approximation with correct asymptotic behavior. *Phys. Rev*. **1988**, *38*, 3098–3100.
15 Lee, C.; Yang, W.; Parr , R.G. Development of the Colle-Salvetti correlation-energy formula into a functional of the electron density. *Phys. Rev.* **1988**, *B37*, 785–789.
16 Grimme, S. Semiempirical GGA-type density functional constructed with a long-range dispersion correction. *J. Comput. Chem*. **2006**, *27*, 1787– 2006.
17 Civalleri, B.; Zicovich-Wilson, C. M.; Valenzano, L.; Ugliengo, P. B3LYP augmented with an empirical dispersion term (B3LYP-D*) as applied to molecular crystals. *Crys. Eng. Comm*. **2008**, *10*, 405–410.
18 Basis set for iodine from TCM CRYSTAL basis set library: M.D. Towler, 1995. http://www.tcm.phy.cam.ac.uk/~mdt26/crystal.html
19 Maschio, L.; Kirtman, B.; Rerat, M.; Orlando, R.; Dovesi, R. Ab initio analytical Raman intensities for periodic systems through a coupled perturbed Hartree-Fock/Kohn-Sham method in an atomic orbital basis. I. Theory. *J. Chem. Phys*. **2013**, *139*, 164101.
20 Zhao, Y.; Truhlar, D.G. The M06 suite of density functionals for main group thermochemistry, thermochemical kinetics, noncovalent interactions, excited states, and transition elements: Two new functionals and systematic testing of four M06-class functionals and 12 other functionals. *Theor Chem Acc*. **2006**, *120*, 215–241. doi:10.1007/s00214-007-0310-x
21 Gatti, C. TOPOND: a program for the application of the quantum theory of atoms in molecules to periodic systems. *Acta Crystallogr*. **1996**, *A52*, 555–556.
22 Gatti, C.; Casassa, S. TOPOND14 User's Manual. 2013. CNR-ISTM of Milano.
23 Kolesov, B.A. How the vibrational frequency varies with temperature. *J. Raman Spectrosc*. **2017**, *48*, 323–326.
24 Kolesov, B.A.; Egorov, N.B. Isotope Effects in Raman Spectra of Crystalline Sulfur α-S_8. *JETP Letters* **2013**, *98*, 134–138.
25 Politzer, P.; Murray, J. S.; Clark, T. Halogen bonding and other σ-hole interactions: a perspective. *Phys. Chem. Chem. Phys*. **2013**, *15*, 11178-–11189.
26 D'amour-Sturm, H.; Holzapfel, W.B. Single crystal x-ray diffraction on iodine up to 5.7 GPa. *Physica* **1986**, *139* & *140B*, 328–329.
27 Buontempo, U.; Filipponi, A.; Martınez-Garcıa, D.; Postorino, P.; Mezouar, M.; Itié, J. P. Anomalous bond length expansion in liquid iodine at high pressure. *PRL*, **1998**, *80*, 1912–1915.
28 Becke, A.; Edgecombe, K. A simple measure of electron localization in atomic and molecular systems. *J. Chem. Phys*. **1990**, *92*, 5397.
29 Silvi, B.; Savin, A. Classification of chemical bonds based on topological analysis of electron localization functions. *Nature* **1994**, *371*, 683−686.
30 Savin, A. Phase transition in iodine: a chemical picture. *Journal of Physics and Chemistry of Solids* **2004**, *65*, 2025–2029.
31 Contreras-García, J.; Marqués, M.; Menéndez, J. M.; Recio, J. M. From ELF to compressibility in solids. *Int. J. Mol. Sci*. **2015**, *16*, 8151–8167. doi:10.3390/ijms16048151